The Cumulus Cell Layer Protects the Bovine Maturing Oocyte Against Fatty Acid-Induced Lipotoxicity 1

Authors: Lolicato, Francesca, Brouwers, Jos F., de Lest, Chris H.A. van, Wubbolts, Richard, Aardema, Hilde, et al.

Source: Biology of Reproduction, 92(1)

Published By: Society for the Study of Reproduction

URL: https://doi.org/10.1095/biolreprod.114.120634

BIOLOGY OF REPRODUCTION (2015) **92**(1):16, 1–16
Published online before print 8 October 2014.
DOI 10.1095/biolreprod.114.120634

The Cumulus Cell Layer Protects the Bovine Maturing Oocyte Against Fatty Acid-Induced Lipotoxicity[1]

Francesca Lolicato,[3] Jos F. Brouwers,[3] Chris H.A. van de Lest,[3] Richard Wubbolts,[3] Hilde Aardema,[4] Paola Priore,[3,5] Bernard A.J. Roelen,[4] J. Bernd Helms,[3] and Bart M. Gadella[2,3,4]

[3]*Department of Biochemistry and Cell Biology, Faculty of Veterinary Medicine, Utrecht University, Utrecht, the Netherlands*
[4]*Department of Farm Animal Health, Faculty of Veterinary Medicine, Utrecht University, Utrecht, the Netherlands,*
[5]*Laboratory of Biochemistry, Department of Biological and Environmental Sciences and Technologies, University of Salento, Lecce, Italy*

ABSTRACT

Mobilization of fatty acids from adipose tissue during metabolic stress increases the amount of free fatty acids in blood and follicular fluid and is associated with impaired female fertility. In a previous report, we described the effects of the three predominant fatty acids in follicular fluid (saturated palmitate and stearate and unsaturated oleate) on oocyte maturation and quality. In the current study, the effects of elevated fatty acid levels on cumulus cells were investigated. In a dose-dependent manner, the three fatty acids induced lipid storage in cumulus cells accompanied by an enhanced immune labeling of perilipin-2, a marker for lipid droplets. Lipidomic analysis confirmed incorporation of the administered fatty acids into triglyceride, resulting in a 3- to 6-fold increase of triglyceride content. In addition, palmitate selectively induced ceramide formation, which has been implicated in apoptosis. Indeed, of the three fatty acids tested, palmitate induced reactive oxygen species formation, caspase 3 activation, and mitochondria deterioration, leading to degeneration of the cumulus cell layers. This effect could be mimicked by addition of the ceramide-C2 analog and could be inhibited by the ceramide synthase inhibitor fumonisin-B1. Interfering with the intactness of the cumulus cell layers, either by mechanical force or by palmitate treatment, resulted in enhanced uptake of lipids in the oocyte and increased radical formation. Our results show that cumulus cells act as a barrier, protecting oocytes from in vitro induced lipotoxic effects. We suggest that this protective function of the cumulus cell layers is important for the developmental competence of the oocyte. The relevance of our findings for assisted reproduction technologies is discussed.

apoptosis, cumulus cells, metabolism, nutrition, oocyte maturation

INTRODUCTION

Oocyte maturation is a complex phenomenon that includes a sequence of events in both the nucleus and cytoplasm of the oocyte and involves the resumption of meiosis [1–3]. Proper oocyte maturation is an essential step for the acquisition of developmental competence once the oocyte is fertilized [2, 4]. Interestingly, a fundamental role in this elaborate process of oocyte maturation is played by the surrounding somatic cells termed cumulus cells [5–7]. Cumulus cells are directly in contact with the oocyte via functional gap junctions through the surrounding zona pellucida [8, 9]. Premature loss of cumulus-oocyte communication impairs bovine oocyte maturation and postfertilization blastocyst development in vitro [10, 11]. While the follicular fluid mirrors the metabolic and ionic composition of the plasma [12], cumulus cells can be considered a barrier between the oocyte cytosol and the follicular fluid. Cumulus cells regulate oocyte metabolism through gap junctions by providing a favorable biochemical microenvironment [13, 14]. A well-studied example of oocyte exposure to an altered metabolic state is represented by negative energy balance (NEB) in the dairy cow [15–17]. During NEB, fertility is compromised. This effect has been associated with increased fatty acid (FA) levels in the circulation and in the follicle due to the mobilization of storage fat from adipose tissues [18].

Regulation of FA exposure and of lipid content of oocytes has been shown to be of importance for oocyte developmental competence and early embryo physiology [19, 20]. Lipids represent an important source of cellular energy, and therefore substantial attention has been paid to lipid metabolism in oocytes and early embryo stages [21, 22]. For instance, lipid content in bovine oocytes tends to increase progressively with oocyte growth [23] while triglyceride (TG) content decreases during in vitro maturation [22], suggesting that neutral lipids may act as an energy source during this process. In the mouse, as in the cow, inhibition of beta-oxidation during oocyte maturation results in decreased blastocyst development [24, 25]. It is well-known that excessive accumulation of lipids also may exert toxic effects on cellular functions (lipotoxicity), especially in cells of nonadipose tissues with limited lipid storage capacity [26, 27]. Lipotoxicity has been correlated with the ability of long-chain saturated FAs to induce accumulation of reactive oxygen species (ROS), nitric oxide [28], diacylglycerols (DAGs) [29], and ceramides [30]. These molecules may generate primary proapoptotic effects on mitochondrial structure or function [31].

Although it has been established that cumulus cells are instrumental for proper oocyte maturation, the adverse effects of elevated FA levels on the cumulus cell layer function [32, 33] is currently not fully understood. In the present study, we have investigated the role of the cumulus cells in protecting the oocyte against FA-induced lipotoxic effects. The in vitro

[1]This work is funded by Pfizer Animal Health.
[2]Correspondence: Bart M. Gadella Department of Biochemistry and Cell Biology, Faculty of Veterinary Medicine, Utrecht University, Yalelaan 2, 3584 CM Utrecht, The Netherlands. E-mail: b.m.gadella@uu.nl

Received: 23 April 2014.
First decision: 23 May 2014.
Accepted: 29 September 2014.

eISSN: 1529-7268 http://www.biolreprod.org
ISSN: 0006-3363

bovine model used in the current study allowed us to closely mimic the effect of elevated FA levels induced by mobilization of storage fat on dominant follicles as observed in vivo [12] and therefore to analyze the responses of cumulus cells to these conditions. The present work aims to give insights into the mechanisms involved in lipotoxic effects induced by saturated FA exposure of cumulus-oocyte complexes (COCs). The relevance of this study for assisted reproduction technology applications in high-yielding dairy cows under NEB symptoms as well as for dietary aberrant women (e.g., patients with anorexia or obesity) is discussed.

MATERIALS AND METHODS

Chemicals and Antibodies

All the chemicals, unless stated otherwise, were obtained from Sigma (Sigma Inc. St. Louis, MO) and were of the highest purity available. Solvents (acetone, acetonitrile, and methanol) were of high-performance liquid chromatography (HPLC) grade (Biosolve, Valkenswaard, The Netherlands). Chloroform was purchased from Roth Chemie GmbH (Mannheim, Germany). Rabbit polyclonal antibody (ab52355 1.13 mg/ml; 1:50 dilution) against perilipin-2 (ADFP), mouse monoclonal antibody (20E8C12 1 mg/ml; 1:50 dilution) against cytochrome c oxidase subunit IV (COX IV), rabbit polyclonal antibody (ab96094 1 mg/ml; 1:50 dilution) against diacylglycerol acyltransferase-2 (DGAT-2) and mouse monoclonal antibody (ab6276) anti beta-actin (AC-15; 1:200 dilution) were purchased from Abcam (Cambridge, United Kingdom). Antibody against cleaved (activated) caspase-3 (Asp175 3.1 mg/ml; 1:50 dilution) (rabbit polyclonal, 9661) was purchased from Cell Signaling Technology (Danvers, MA). Nuclear staining reagent TO-PRO-3 iodide (642/661) and secondary antibodies Alexa Fluor 488 (1 mg/ml; 1:200 dilution), Alexa Fluor 568 (1 mg/ml; 1:200 dilution), and Alexa Fluor 647 (1 mg/ml; 1:200 dilution) were purchased from Life Technologies (Carlsbad, CA).

Collection of Oocytes

Bovine ovaries were collected from a local abattoir and transported to the laboratory within 2 h after dissection. Follicles ranging from 3–8 mm were aspirated under low vacuum by a suction pump, and COCs with a minimum of three layers of cumulus cells were selected and cultured in supplemented M199 maturation medium (Gibco, Life Technologies, Carlsbad, CA) as previously described [19]. The oocytes were matured in groups of 35 COCs and incubated under a humidified atmosphere of 5% CO_2 in air for 23 h at 39°C. For all COCs collected as well as for denuded oocytes, the morphology was scored under a differential interference contrast (DIC) microscope (Leica Microsystems GmbH, Wetzlar, Germany).

Fluorescent FA Analog Incorporation into Neutral Lipids of Maturing Oocytes

Maturing oocytes were incubated in M199 maturation medium supplemented with 6 μM Bodipy 558/568 C12 (fluorescent FA analog, BODIPY-FA) (Molecular Probes, Eugene, OR) in the presence or absence of the cumulus cells for 4 h to test the role of cumulus cells in FA uptake at the beginning of the in vitro maturation. For imaging purposes, the cumulus cell layers of intact COCs were mechanically removed post-BODIPY-FA incorporation by mouth controlled handmade pipettes with an inner diameter of about 200 μm [34]. Both type of denuded oocytes were fixed with 4% paraformaldehyde, and the neutral lipid fraction contained in the lipid droplets (LDs) was counterstained with Bodipy 493/503 probe (BODIPY-LD; Molecular Probes) as previously described in Aardema et al. [19]. The fluorescence signals were detected by confocal microscopy (Zeiss/Bio-Rad, Hertfordshire, United Kingdom).

In Vitro Maturation and Treatments

COCs were exposed either to palmitate (PA), stearate (SA), or oleate (OA) at a concentration of 0 (control group) or 250 or 500 μM FA in M199 maturation medium or to an equimolar mixture (250 μM of each FA) of SA + OA or PA + OA during the entire maturation period of 23 h. Three additional groups of COCs were exposed to either 500 μM PA, 500 μM SA plus 50 μM fumonisin-B1 (FB1), the inhibitor of the de novo ceramide synthase [35], or 100 μM ceramide-C2 (Calbiochem-Merck, Bad Soden, Germany). FAs were complexed to delipidated bovine serum albumin as described by Aardema et al. [19] and the final FA concentrations used in the experiments were based on in vivo measurements of individual and total FA content in follicular fluid [12]. Stock concentrations of FB1 or ceramide-C2 were dissolved in dimethylsulfoxide, and the final concentrations used were based on Yuzefovych et al. [36]. Control cultures not treated with FB1 and ceramide-C2 received the same concentration of dimethylsulfoxide as in the compound-treated cultures.

Accumulation of ROS in COCs

COCs immediately after collection were incubated in M199 maturation medium supplemented with 5 μm 2′,7′-dichlorodihydrofluorescin diacetate (DCHF-DA) (a cell-permeable fluorogenic probe) (OxiSelect Intracellular ROS Assay Kit; Cell Biolabs Inc., San Diego, CA) under humidified atmosphere of 5% CO_2 in air for 1 h at 39°C in order to preload the cells with the DCHF-DA probe. Subsequently, cells were washed three times in Hepes-buffered M199 (Gibco, Life Technologies) to remove excess probe and cultured in M199 maturation medium under control condition and with different FAs or reagents as previously described. Hydrogen peroxide was used as a positive control of the ROS assay, according to the manufacturer's protocol. In each experiment, a group of 35 COCs was cultured in the final hour of the in vitro maturation in presence of 1000 μM hydrogen peroxide. A total of 411 COCs were used for the ROS assay in at least three independent runs, and the fluorescence signal reflecting intracellular ROS levels was detected by confocal microscopy (Zeiss/Bio-Rad). Because the conversion of DCHF-DA to DCHF is dependent on esterase activity and precedes further oxidation to highly fluorescent 2′,7′-dichlorodihydrofluorescein by ROS, parallel experiments to quantify esterase activity in oocytes were performed with fluorescein diacetate (FDA) [37]. To measure esterase activity, COCs were collected after 23 h of maturation under control condition or in the presence of 250 μM OA, 500 μM PA, 100 μM ceramide-C2, or hydrogen peroxide (1 h, 1 mM), denuded, and incubated in PBS for 15 min in the presence of 0.12 μM FDA (20 oocytes were measured per treatment). A second pool of oocytes after exposure to the same treatments (20 oocytes per treatment) was incubated with DCHF-DA for detection of fluorescent probe intensities. An additional group of immature oocytes (control germinal vesicle; CTR-GV) was added to the experiment in order to measure both the esterase activity and the ROS signal before the treatments (20 oocytes). FDA fluorescent signal reflecting esterase activity and 2′,7′-dichlorodihydrofluorescein fluorescence signal indicating intracellular ROS levels were detected by confocal microscopy (Zeiss/Bio-Rad). Mean intensities of the labels within the area of the oocytes were measured in uncorrected images using a customized macro written in FIJI and available for download at bc-uu.nl/cci. The fluorescence signals are expressed in arbitrary units per oocyte.

Immune Fluorescent Staining

Immune labeling of COCs was performed as previously described in Aardema et al. [19]. Briefly, fixed and permeabilized COCs were incubated with a 1:50 dilution of rabbit polyclonal antibody against perilipin-2 or mouse monoclonal COX IV. As negative controls, purified mouse or rabbit immunoglobulin G (BD Biosciences, San Jose, CA) matching the host species of the primary antibodies was used, and the dilutions of the negative controls were identical to the dilutions of the primary antibodies used in the same experiment. COCs were stably positioned on a 0.12-mm eight-well Secure-Seal Spacer (Molecular Probes) on a glass slide (Superfrost Plus; Menzel, Braunschweig, Germany) and mounted in a drop of Vectashield (Vector Laboratories, Inc., Burlingame, CA). In this study, an average of 20 matured COCs for treatment and for each protein was imaged in three independent experiments.

Confocal Microscopy

Confocal microscopy was performed by using a Bio-Rad Radiance 2100 MP setup (Zeiss/Bio-Rad) attached to a Nikon Eclipse TE300 inverted microscope (Nikon, Badhoevedorp, The Netherlands) with a 40× magnification (1.25 NA) oil immersion objective. Images were acquired using LaserSharp 2000 software (Zeiss/Bio-Rad). Metaphase-II oocytes (from anaphase-I up to metaphase-II plate) were selected on the basis of the nuclear stage by using TO-PRO-3 Iodide 642/661 staining. The 8-bit grayscale images of each oocyte were processed with FIJI software (available for download at http://pacific.mpi-cbg.de/wiki/index.php/Fiji) by applying the following commands: median filter, (radius 1.0 pixels), background subtraction (rolling ball radius 150.0 pixels). DIC images and COX IV immune-labeling images were captured with a Leica TCS SPE II confocal system (Leica Microsystems GmbH, Wetzlar, Germany).

Image Analyses and Fluorescent Signal Quantification

ROS fluorescent signal quantification in the different experimental conditions was correlated with the perilipin-2 fluorescent signal. ROS signals were low and less confined compared to perilipin-2 signals, but by measuring the ratio of ROS and perilipin-2 label within a grid of rectangular region of interest (ROI) in the oocyte images (taken at the midregion of the oocyte), correlation between ROS signal and stained LDs could be made. Mean intensities of the labels within these ROIs were measured in uncorrected images using a customized macro written in FIJI (available for download at bc-uu.nl/cci). Measuring relative LD area within the oocytes was performed using a customized script (available for download at bc-uu.nl/cci) in Cell Profiler (available for download at http://www.cellprofiler.org) [38]. Oocyte outlines were determined based on the cumulative fluorescence images, while LD regions were isolated based on BODIPY-LD staining. Relative lipid areas to the imaged oocyte area were determined by calculations in Excel (Microsoft, Redmond, WA).

Immunoblotting

Matured oocytes were completely denuded by mouth pipetting, and cumulus cells were collected separately. Cumulus-free oocytes and corresponding cumulus cells were directly lysed in an appropriate amount of lithium dodecyl sulfate-loading buffer (Invitrogen, Carlsbad, CA) in presence of 0.1 M dithiothreitol. For protein detection (perilipin-2, DGAT-2, or COX IV), an average of 60 oocytes per lane, corresponding to approximately 6 μg of total protein [39], and related cumulus cells were used. The signals were visualized by enhanced chemiluminescence using a Gel Doc XR system and analyzed with Quantity-One 4.6.3 Image software (Bio-Rad, Hercules, CA). The membranes were subsequently probed with mouse monoclonal anti-beta-actin to normalize the results.

Extraction and Isolation of Neutral Lipids

The total lipid fractions from oocytes as well as their corresponding cumulus cell layers dissected from COCs were extracted according to the method of Bligh and Dyer [40] starting with 200 μl aqueous phase. Internal standards for TG and free cholesterol (Chol)—tripentadecanoin and 3 keto-sterol (Larodan Fine Chemicals, Malmö, Sweden), respectively—were included during the extraction to calculate the recovery and absolute concentrations. Subsequently, TG, DAG, Chol, cholesteryl esters, and ceramides (henceforth referred to as the neutral lipid fraction) were separated from phospholipids by solid-phase extraction on silica gel 60 (Merck, Darmstadt, Germany) minicolumns made in-house based on Rouser et al. [41]. The neutral lipids fraction was eluted with three volumes of acetone [42], dried under a constant stream of nitrogen gas at 40°C, and stored at −20°C until use [41].

HPLC-Mass Spectrometry Analysis of Neutral Lipids

Isolated neutral lipids were dissolved in 25 μl of methanol/chloroform (1:1, v/v) and 20 μl was injected on a HALO C8 (150 × 3.0 mm, particle size of 2.7 μm) HPLC column (Advanced Material Technology Inc., Wilmington, DE) maintained at 40°C. Lipids were eluted by a linear gradient from methanol/water (1:1, v/v) to methanol/2-propanol (4:1, v/v) in 5 min, followed by isocratic elution with the latter solvent for 20 min and regeneration of the column for 5 min, all at a flow rate of 0.3 ml/min. The column effluent was introduced by an atmospheric pressure chemical ionization interface into a 4000 QTRAP mass spectrometer (Applied Biosystems/AB Sciex Instruments, Toronto, ON, Canada). The mass spectrometry settings were optimized by recording the total lipid profile of bovine oocytes and their cumulus cells in full-scan positive ion mode (scan range, m/z 250–1100 amu). Full-scan data were recorded in ion-trapping mode. Based on these results (data not shown), the mass spectrometer was then operated in multiple reaction-monitoring mode at unit mass resolution (for selected mass transitions see Supplemental Table S1; Supplemental Data are available online at www.biolreprod.org). The source temperature was set to 450°C, and nitrogen was used as the curtain gas. The declustering potential was set to 100 V and the needle current to 3 μA. Ions were identified by the automated acquisition of product ion spectra (from m/z 200 to m/z 650 amu) in a separate HPLC run using a collision energy of 32 V for the TG, 35 V for Chol, and 38 V for ceramides. Peaks were identified by comparison of retention time (t_R) and (product) mass spectra with authentic standards and calibration curves of synthetic analogs of identified compounds.

Data Processing and Statistics

Data were recorded with Analyst v1.4.2 software (MDS Sciex, Concord, ON, Canada) and exported to mzXML format. Peak detection, integration, and alignment were performed using the open source software package XCMS version 1.22.1 running under R version 2.72 (R development Core Team, 2011, available for download at http://www.R-project.org/) [43]. Zero values, in samples with missing peaks, were prevented by forced integration at the calculated expected t_R of the peak. Principle component analysis (PCA) was performed using the PCA methods package (pcaMethods) [44]. The attribution of the third FA on the glycerol backbone for the exact determination of TG species was performed by deconvolution of FA composition on the linear relation that exists between the t_R and the carbon number (CN) minus the degree of saturation (UN) accordingly to the equation $t_R \cong 14.2 + 0.046(CN - 1.45 \times UN)$ empirically derived from $t_R \cong CN - 1.45 \times UN$. For lipidomic data, the statistical analysis was performed using R statistical software version 2.72. Fluorescent signal quantification was analyzed with a one-way ANOVA, using the IBM SPSS 20 software (available for download at http://www-01.ibm.com/software/analytics/spss/). All the measures are reported as mean ± standard deviation (SD). A chi-squared test was performed for the statistical analysis of COCs morphology. Values of $P < 0.05$ were considered statistically significant.

RESULTS

Cumulus Cells Regulate the Supply of FA to the Oocyte

The role of cumulus cells in FA uptake was investigated by labeling living in vitro maturing COCs with the fluorescent FA analog BODIPY-FA (Fig. 1). This analog has previously been used to examine FA uptake in mammalian cells and yeast [45, 46]. Oocytes cultured in the presence of their cumulus cell layer showed only low levels of FA incorporation after 4 h of in vitro maturation (Fig. 1A). Mechanical removal of the cumulus cell layer before administration of BODIPY-FA significantly increased the incorporation rate of the FA analog (Fig. 1A). Note that the differences in total neutral lipid staining as depicted in Figure 1A with BODIPY-LD is due to variation in LD amount and size between individual oocytes and is independent from cumulus removal and/or the BODIPY-FA incorporation period. Quantification of the BODIPY-FA-stained area fractions of the oocyte images are shown in Figure 1B. Within 4 h in denuded oocytes, the uptake of BODIPY-FA was already >60% of the levels observed after 23 h incorporation (Fig. 1B). Incorporation of BODIPY-FA in intact COCs during the first 4 h incubation period and at 23 h was <25% of that of denuded oocytes (Fig. 1B).

FA Are Effectively Stored into LDs of Cumulus Cells

The lower efficiency of FA incorporation in oocytes in the presence of the cumulus cells (Fig. 1B) indicates that the cumulus cells actively modulate FA supply to the oocyte. One possibility is that exogenous FAs are absorbed by cumulus cells and stored as TGs into the LDs. Therefore, we investigated the effect of the supplementation of the three most abundant FAs in follicular fluid of cows, that is, PA, SA, and OA [12], on the lipid storage capacity of COCs. After the FA incubation, COCs were immune labeled for the LD-specific PAT protein perilipin-2 [47] (Fig. 2A). Incubation with OA, PA, and SA strongly increased the amount of perilipin-2-decorated LDs in the cumulus cells while the interior of the oocyte did not show a rise in staining after the FA addition (Fig. 2A). Note that during PA incubations, despite the induced deterioration of the corona radiata, the remaining cumulus cells were still able to store PA (Fig. 2A, panels V/VI) as is reflected in the highly increased amount of LDs and concomitant higher perilipin-2 labeling (for corresponding neutral lipid content and composition responses to the diverse conditions, see Supplemental Figs. S1 and S2).

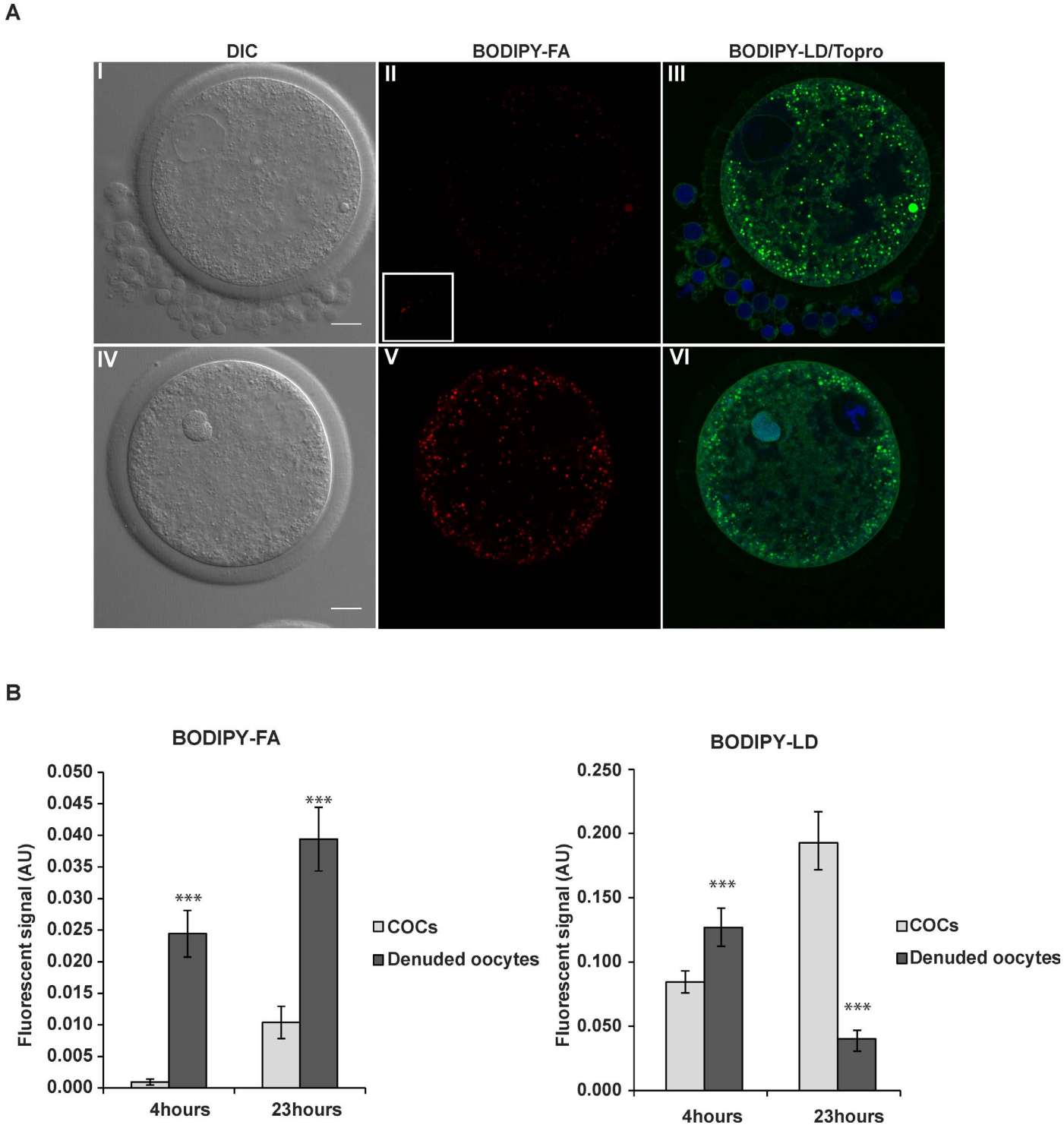

FIG. 1. Fluorescent FA analog transport and incorporation into LDs of the oocyte. Bovine oocytes were matured in vitro for 23 h in presence of 6 μM red fluorescent FA analog BODIPY-FA with the cumulus cells or after their manual removal. Cells were collected at 4 and 23 h, denuded from cumulus cells, and analyzed for FA incorporation. **A**) Incorporation of BODIPY-FA probe was followed in maturing oocytes after 4 h of in vitro maturation with (**I**–**III**) or without (**IV**–**VI**) cumulus cells. The small quadrant of **II** shows higher detail of the few cumulus cells left. Neutral lipid counterstaining for all present LDs was done with the green BODIPY-LD probe (**III**–**VI**) and indicated that the BODIPY-FA analog (**II** and **V**) was incorporated and stored as esterified lipids in LDs of the oocyte. For clarity, the differences in total neutral lipid (BODIPY-LD; green) staining of panels **III** and **VI** are due to preexisting variability in LD amount and size in individual oocytes. The differences in amount of incorporated BODIPY-FA analog (red, visualized in **II** and **V**) are due to different rates of conversion of the FA analog into neutral lipids. Nuclei are stained in blue with TO-PRO-3 (**III**, **VI**). DIC images of both conditions are shown in **I** and **IV**. Bar = 20 μm. **B**) BODIPY-FA and BODIPY-LD fluorescent signal quantitation in COCs at 4 and 23 h of in vitro maturation. Values represent the mean ± SD of BODIPY-FA (left panel) or BODIPY-LD (right panel) fluorescent signals of 30 oocytes per group. Statistical analysis performed with one-way ANOVA test confirmed a significant difference among the two groups (COCs and denuded oocytes) in the two time points (4 and 23 h) for the two probes (***$P \leq 0.001$).

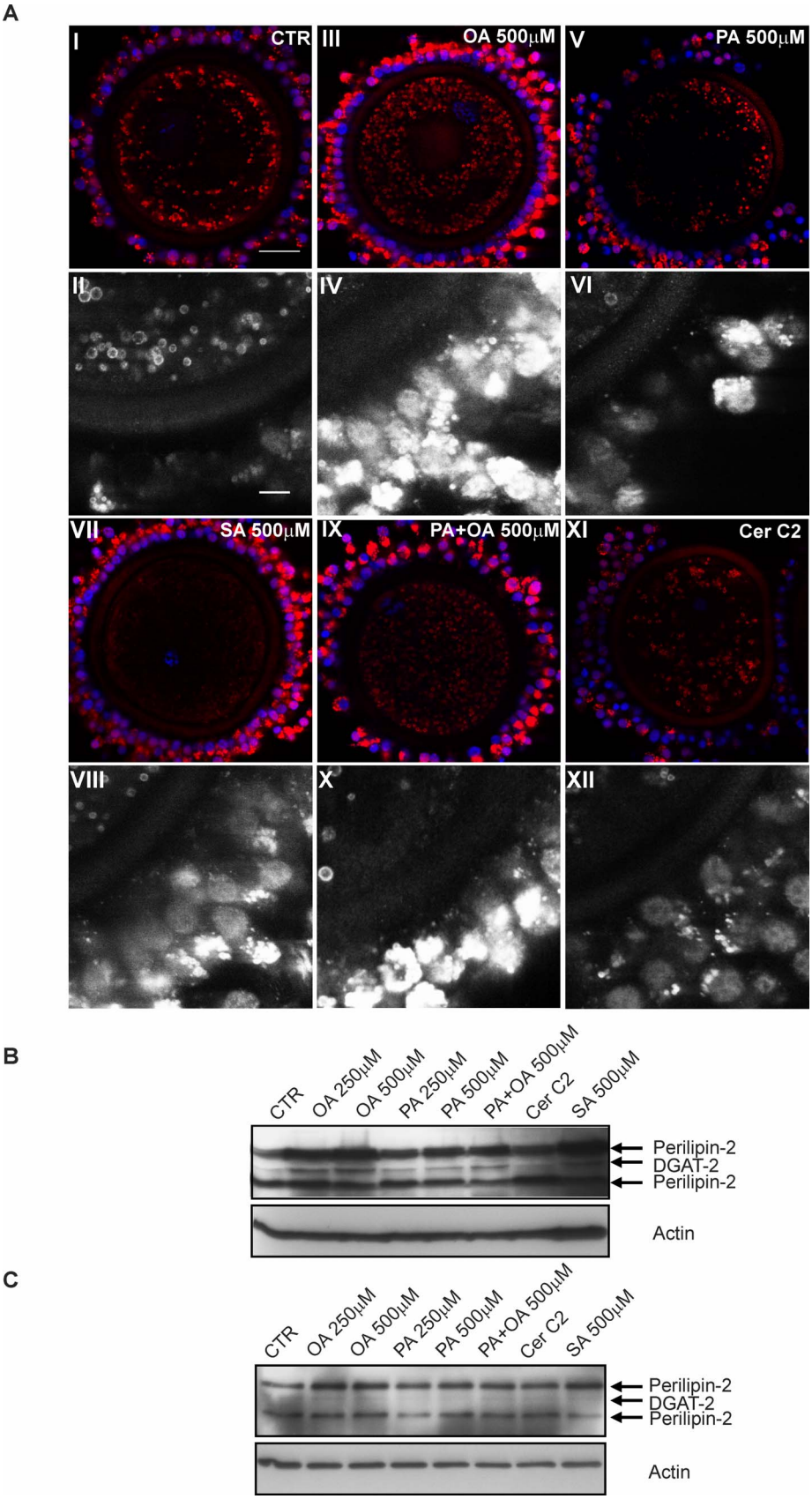

FIG. 2. FA incorporation into the LDs of COCs. **A**) Immunofluorescence of COCs after 23 h of in vitro maturation in the following conditions: **I** and **II** control (CTR, no FA addition), **III** and **IV** with 500 μM OA, **V** and **VI** with a 500 μM PA, **VII** and **VIII** with 500 μM SA, **IX** and **X** with 500 μM PA + OA (1:1, molar ratio), **XI** and **XII** with no FA addition but in presence of 100 μM ceramide-C2 (Cer C2). Unpaired number panels depict perilipin-2 (red) and TO-PRO-3 (blue) labeling. Bar = 20 μm. The corresponding paired number panels depict perilipin-2 labeling of cumulus cells details; bar = 5 μm. **B**, **C**) Western blot analysis: immune detection of perilipin-2 and DGAT-2 in cumulus cells (**B**) and oocytes (**C**). COCs matured in control condition and under FA supplementation were dissected and protein extracts from 60 oocytes per each lane or the corresponding dissected cumulus cell layers were loaded on a gel. Actin was used as loading control. CTR, control; OA, oleate; PA, palmitate; SA, stearate; cer C2, ceramide-C2.

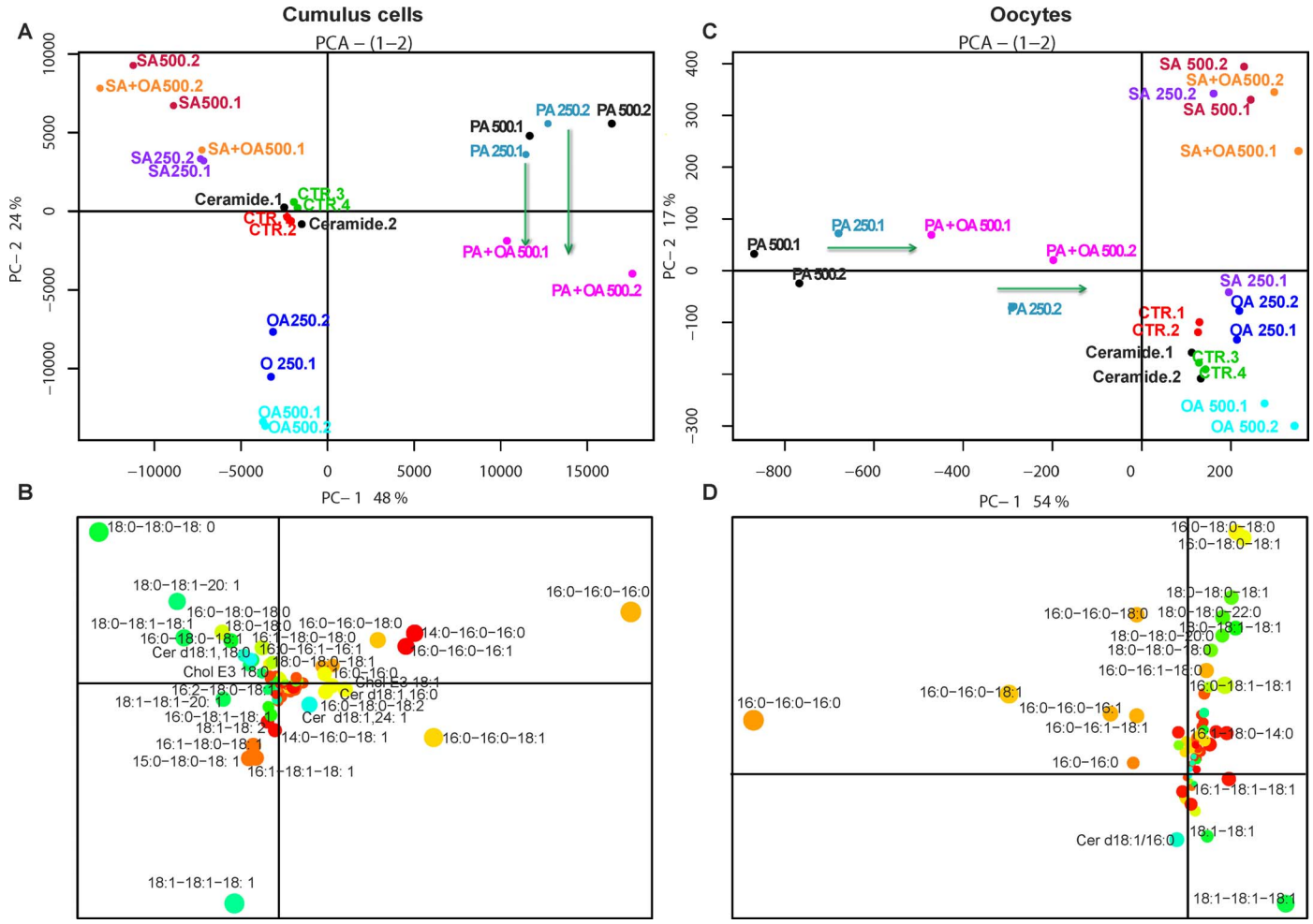

FIG. 3. Lipid composition of COCs after maturation in FA-enriched media. **A**–**D**) Principal component analysis (PCA) on the lipidome of dissected cumulus cells (**A**, **B**) and oocytes (**C**, **D**) from COCs exposed to elevated levels of specific FAs. Cells were incubated in the absence of FA (control [CTR]) or in presence of SA, PA, OA alone, a mix (PA + OA or SA + OA), or in presence of ceramide-C2 (Cer C2) in the concentrations indicated (in μM) in **I** and **II** and specified in *Materials and Methods*. **A** and **C** show the score plots of the PCA (duplicates are indicated by suffix 1 and 2, respectively), whereas **B** and **D** show the corresponding loadings of individual lipid species as they contribute to the score plots of cumulus cells (left) and oocytes (right), respectively. Note that elevated levels of OA, PA, and SA induce specific, dose-dependent and reproducible changes in the neutral lipidome compared to CTR conditions. Arrows indicate the effect of 250 μM OA in the presence of 250 μM PA when compared to 250 μM PA alone. No effects were noted for 250 μM OA in the presence of 250 μM SA when compared to 250 μM SA alone ($P < 0.001$ for cumulus cells and $P < 0.004$ for oocytes). CTR, control; OA, oleate; PA, palmitate; SA, stearate; cer C2, ceramide-C2; FB1, fumonisin-B1.

Immunoblot analysis showed to some extent an increase in perilipin-2 protein expression in the cumulus cell layers upon addition of FAs (Fig. 2B) while this increase was not observed in the corresponding oocytes (Fig. 2C). We do not have an explanation for the discrepancy between moderate increase of perilipin-2 expression on immunoblot when compared to the high up-regulation of the immunofluorescence signal. Speculatively, it is possible that the binding epitope of perilipin-2 becomes in some way better exposed to its antibody under the induced neutral lipid storage conditions of the cumulus cells, that is, increasing amounts of neutral lipids (see also Supplemental Figs. S1 and S2). Support for this notion comes the finding that OA, PA, and SA induced increased levels of DGAT-2 in cumulus cells (Fig. 2B), thus increasing neutral lipid storage as a result of increased TG production by this enzyme. On the other hand, DGAT-2 activity was below the threshold detection level in the oocytes (Fig. 2C). Equimolar levels of OA and PA gave similar results (Fig. 2). These results suggest that cumulus cells actively incorporate the increased levels of exogenous FAs (as is shown in Supplemental Figs. S1 and S2) and thus may act as a barrier that enables regulation of FA exposure to the oocyte. Beyond this, we noted that oocytes matured in the presence of PA showed preferential accumulation of perilipin-2-positive LDs at sites where cumulus cell protection was lost (Fig. 2A). As a negative control, ceramide-C2 analog was added to the control medium (without FA addition) and the maturing COCs did not show increased perilipin-2 immunofluorescence (Fig. 2A), increased levels of DGAT-2 (Fig. 2, B and C), or increased neutral lipid synthesis (Supplemental Figs. S1 and S2).

Lipidomic Analysis of Neutral Lipids Stored in LDs of Cumulus and Oocytes

The accumulation of neutral lipids in cumulus cells and oocytes was confirmed by lipidomic analysis. COCs were exposed to different FAs during in vitro maturation and subsequently processed for lipidomic analysis. PCA of the obtained data (Fig. 3) showed that the COCs reacted in a dose-dependent manner to the administered FA and that the neutral lipid composition of the resulting cumulus cells (Fig. 3, A and B) and oocytes (Fig. 3, C and D) were different for each

administered FA. This was predominantly due to the fact that the cumulus cells induced incorporation of the administered FAs into TGs. Hence, the resulting increase in TG levels reflected an increase in TG species that contained one or more of the exogenously added FA(s) (see Supplemental Fig. S1, A and B, for quantitation of individual TG species in cumulus cells and oocytes, respectively, and Supplemental Fig. S2 for comparison quantitation of total TGs and other neutral lipids under various experimental conditions). For example, TG species with three PAs, SAs, or OAs were the most discriminating component in the PCA (see Fig. 3, B and D, loading plots), indicative for incubations with PA, SA, and OA (Fig. 3, A and C). Likewise, 250 μM OA in combination with 250 μM PA had the combined effect of each of the two FAs (shown as arrows in Fig. 3, A and C) both in oocytes and cumulus cells while 250 μM OA in combination with 250 μM SA did not elicit additional effects when compared to 250 μM SA alone (Fig. 3). Principle component (PC) comparison of the responsiveness of cumulus cells and oocytes to exogenous FAs revealed that oocytes were more responsive to PA: in the lipidomic analyses of oocytes, PC-1 explains 54% of the variance in the neutral lipid levels, and only PA addition caused a remarkable left shift in PC-1 as compared to the matured control oocytes (Fig. 3). As expected for PC-1, the (16:0, 16:0, 16:0) TG, (16:0, 16:0, 18:0) TG, and (16:0, 16:0, 18:1) TG were the dominant TG molecular species explaining this variance. Oocytes treated with SA and/or OA did not vary with respect to PC-1 but did vary with respect to PC-2 from control matured oocytes, which explained only 17% of the variance. In contrast to these observations in oocytes, both saturated FAs (PA and SA) caused a strong shift in PC-1 as compared to the matured control cumulus cells (Fig. 3). Cumulus cells treated with OA did not vary in PC-1. From these data, it can be concluded that cumulus cells are most responsive to saturated FAs and less responsive to OA. Almost all the duplicates gave similar responses with the exception of the low SA dose (250 μM) oocyte samples. In one experimental group, a similar response as was reported for the 500 μM dose was recorded, while in the other, the PC-2 response was not present (Fig. 3C). The corresponding cumulus cells both gave at the 250 μM dose reproducible and expected intermediate responses when compared to control oocytes and to oocytes exposed to the 500 μM SA dose (Fig. 3A). The variety in responses of the two oocyte groups may be due to the fact that the 250 μM SA condition was not affecting the cumulus mass to the extent that oocyte responses were elicited. As a consequence, some oocytes remained under protection whereas others did not. At the 500 μM dose, however, all the cumulus layer protection against SA was diminished.

Another interesting observation was that in all the incubations containing PA, an elevation of ceramide levels could be detected in the cumulus cells as well as in the oocytes (Fig. 4). In cumulus cells (Fig. 4A), ceramide levels increased more under the conditions tested, which was also reflected by higher increases in ceramide levels upon the addition of PA in cumulus cells (40–100 pmol/cumulus cells from one oocyte) as compared to oocytes (1–5 pmol/oocyte) (Fig. 4B). Similar responses were observed for glucosylceramides in cumulus cells and oocytes (Supplemental Fig. S3). Ceramide species do not seem to be directly involved in neutral lipid storage because exogenous administration of ceramide-C2 did not affect the composition nor the amount of TG storage (Supplemental Fig. S2). As mentioned above, this is in line with the observation that ceramide-C2 addition to COCs did not result in increased DGAT-2 levels or in accumulation of LDs (Fig. 2). On the other hand, 250 μM OA and 250 μM PA together produced a dramatic shift in the neutral lipid profile when compared to 250 μM PA alone (Fig. 3A) while both treatments caused a similar increase in ceramide levels, showing again that the two responses were independent of each other (Fig. 4A). Also, ceramide-C2 treatment only caused ceramide production in oocytes, whereas this response was not observed in cumulus cells (Fig. 4). Although we do not have a good explanation for this discrepancy, we keep the possibility open that the oocyte is protected from naturally occurring (water-insoluble) ceramides by cumulus cells as was reported for FAs. However, the artificial water solubility and membrane permeability of ceramide-C2 (caused by its short C2-FA chain) may allow unprotected passive diffusion of ceramide-C2 into the oocyte. Ceramide-C2 treatment also led to the deterioration of the cumulus layers of COCs (Figs. 5E and 6). Therefore, both the passive diffusion properties of ceramide-C2 as well as the disruption caused to the cumulus cell layer is believed to lead to direct exposure of the oocyte to ceramide-C2 during the maturation. The absence of ceramide formation in the cumulus may be related to the deterioration of these cells by ceramide-C2 or to different ceramide metabolism/signaling responses between cumulus cells and the oocyte.

PA and Ceramide-C2 Cause ROS Formation and Cumulus Cell Layer Deterioration

Cumulus cell expansion is considered to be a hallmark of oocyte maturation [14]. Previous studies on human granulosa cells [48] and rat Leydig cells in vitro [49] demonstrated the induction of apoptosis by PA and SA probably through ceramide production and indicated that PA inhibited bovine granulosa cell steroidogenesis and proliferation in vitro [18]. Because our results revealed an increase in ceramide production during incubation of COCs with PA (Fig. 4), the influence of exogenous FAs and the role of ceramide on structural properties of cumulus cell layers were determined. To this end, the effects of FA administration to COCs were compared to COC treatment with ceramide-C2, a proapoptotic stimulus known to mediate its effect via ROS (Fig. 5). We used hydrogen peroxide as a positive control for ROS-mediated induction of cumulus deterioration. Cumulus cell layer integrity was analyzed using DIC microscopy, and intracellular ROS production was determined using a prelabeling treatment with DCHF-DA (Fig. 5). DCHF-DA prelabeled COCs cultured under control conditions or in the presence of OA showed an intact cumulus with low ROS formation (Fig. 5A–D). Quantitation of cumulus intactness showed that 74%–82% of the COCs remained intact and 67%–75% of the COCs did not show signs of ROS production (Table 1). However, in the presence of PA, SA, hydrogen peroxide, or ceramide-C2, less than 50% of the cumulus cell layers remained intact with concomitant high levels of ROS in oocytes with deteriorated cumulus cells (Fig. 5 and Table 1). Interestingly, addition of 250 μM PA in combination with 250 μM OA reduced cumulus deterioration and reduced peroxidation of DCHF-DA in the COCs (Table 1 and Fig. 5, K and L). The ROS production in the oocyte correlated highly with the degree of deterioration of the cumulus (Table 1), and the conditions that significantly induced both signs of deterioration are indicated in Table 1 (for statistics, see Supplemental Table S2). The involvement of ceramides in PA-mediated ROS production and cumulus cell deterioration was further investigated using FB1, a specific inhibitor of ceramide synthase. Indeed, coincubation of SA or PA with FB1 markedly reduced the deterioration of the cumulus cell layer and the peroxidation of DCHF-DA in the

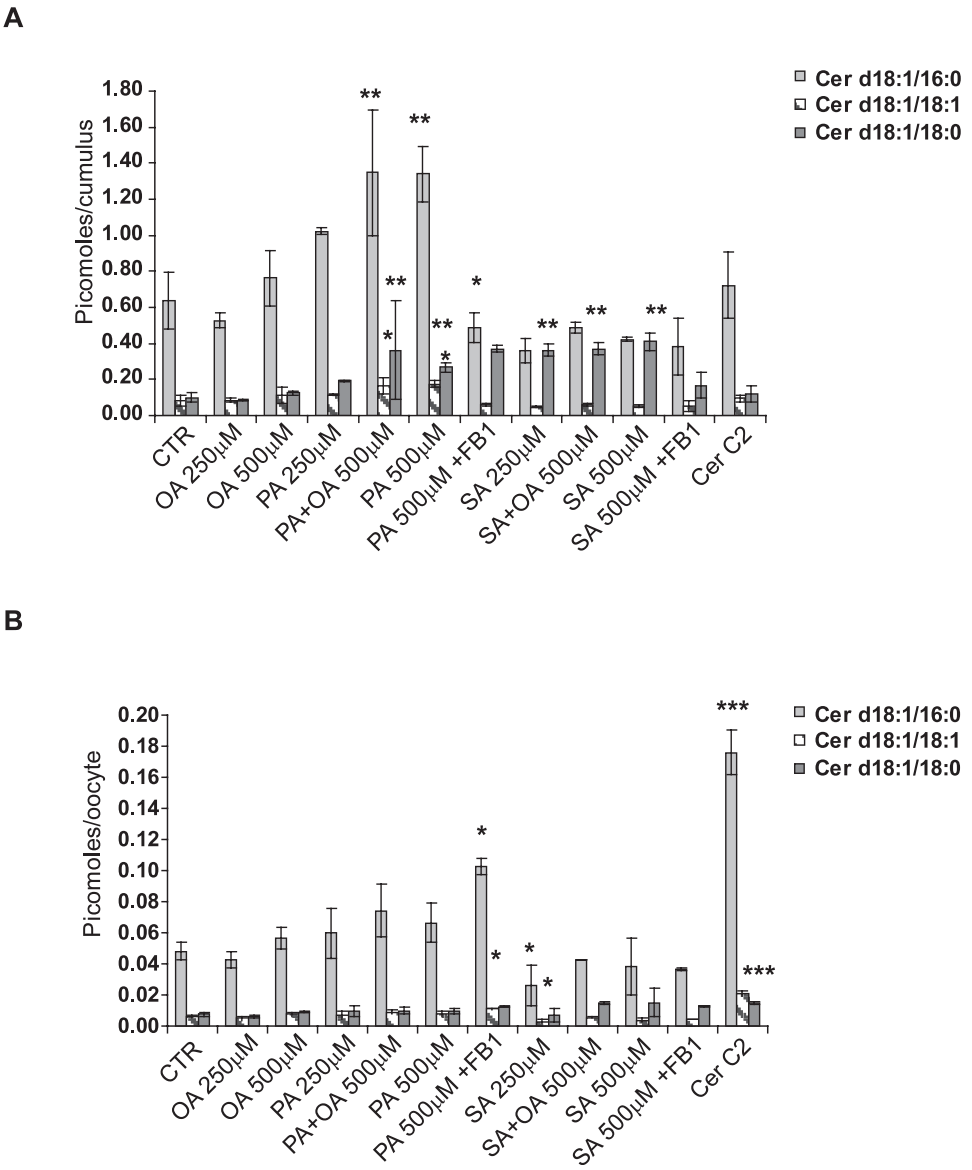

FIG. 4. Lipidomic analysis of ceramide content in cumulus cells and oocytes**.** Multiple reaction monitoring analysis allowed the detection of 11 selected ceramides. Among them, dihydroceramides (first the sphinganine chain length is indicated with d, followed with the *N*-acyl chain length) d18:1/16:0, d18:1/18:1, and d18:1/18:0 resulted to be the most abundant species. Ceramides d18:1/16:0, d18:1/18:1, and d18:1/18:0 quantitation in cumulus cells pool per oocyte (**A**) and single oocyte (**B**) matured under different treatments was determined as specified in *Materials and Methods*. Recovery and absolute concentrations were calculated on the basis of the internal standards and by comparison with the standard curve, respectively. Cumulus cells values were normalized per Chol content; oocytes values were divided by the number of the oocytes in each sample. Values represent the mean ± SD of about 30 oocytes or cumulus cell layers per treatment processed in duplicate. $^{*}P \leq 0.05$, $^{**}P \leq 0.01$, and $^{***}P \leq 0.001$ were determined by post hoc test and were considered significantly different from the control. CTR, control; OA, oleate; PA, palmitate; SA, stearate; cer C2, ceramide-C2; FB1, fumonisin-B1.

COCs (Table 1, Supplemental Table S2, and Fig. 5, S, T, W, and X). The efficacy of FB1was determined by lipidomic analysis, confirming inhibition of ceramide production in cumulus cells and oocytes in the presence of PA (Fig. 4, A and B). Because the fluorescence levels detected by oxidized DCHF are dependent on deacetylation of DCHF-DA by esterase activity, a direct esterase activity assay was performed using quantification of deacetylated FDA as described by Morado et al. [37] (Fig. 6). Compared to the GV oocytes (used as a preloading control for ROS experiments described above), an increase in FDA signal was noted in all matured oocytes (Fig. 6A). However, no significant differences in esterase activities were detected between oocytes that were matured under control condition or in presence of either OA or hydrogen peroxide (Fig. 6A). Interestingly, oocytes matured in the presence of a high concentration of PA or ceramide-C2 had lower esterase activity (Fig. 6A). However, the PA- or ceramide-C2-matured oocytes showed a marked and significant increase in ROS-dependent conversion of the DCHF-DA probe when compared to all the other conditions (Fig. 6B). This implies that our preloading strategy of COCs was sufficient to load the cells with proper amounts of DCHF and to enable the detection of oxidative stress-dependent probe conversion into the fluorescent state.

Triple-labeling experiments allowed us to determine the subcellular localization of ROS production. To this end, COCs were matured in the absence (control) or presence of OA, PA, or ceramide-C2. Subsequently, COCs were stained for ROS

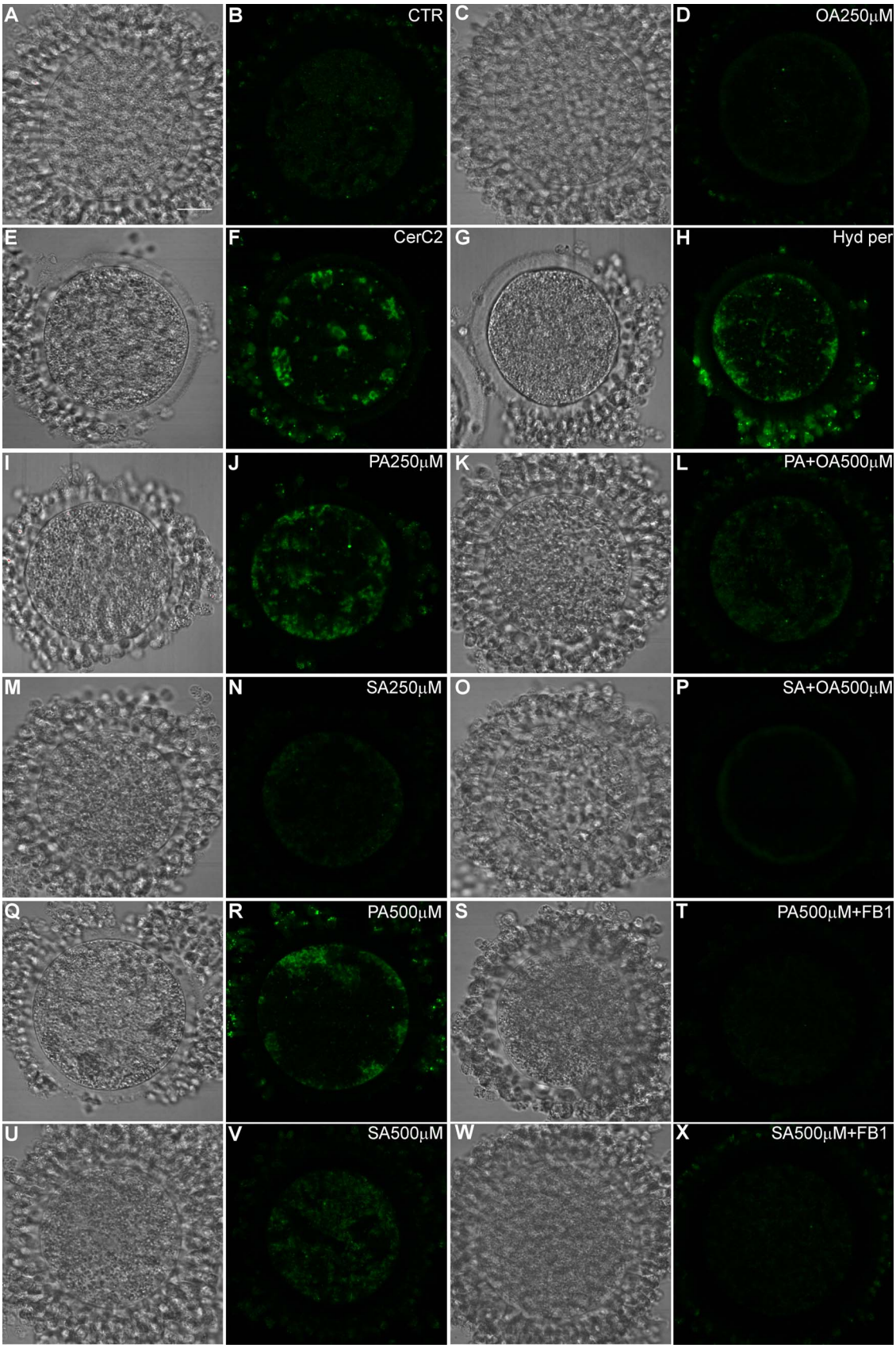

FIG. 5. ROS formation in COCs after 23 h of in vitro maturation. Paired micrographs of COCs with phase contrast microscopy (left row and third row) and corresponding oxidized DCHF-DA fluorescence (green) (second row and right row) are provided under diverse maturation conditions at 23 h: control (CTR) with no FA addition (**A**, **B**); with 250 μM OA (**C**, **D**); with 100 μM ceramide-C2 (**E**, **F**); with 1 mM hydrogen peroxide (hyd per) (**G**, **H**); with 250 μM PA (**I**, **J**); with 500 μM PA + OA (1:1, molar ratio) (**K**, **L**); with 250 μM SA (**M**, **N**); with 500 μM SA + OA (1:1, molar ratio) (**O**, **P**); with 500 μM PA (**Q**, **R**); with 500 μM PA + 50 μM FB1 (**S**, **T**); with 500 μM SA (**U**, **V**); or with 500 μM SA + 50 μM FB1 (**W**, **X**). Bar = 20 μm. For each condition, a representative COC morphology and DCHF-DA oxidation labeling is represented ($n > 12$). CTR, control; OA, oleate; PA, palmitate; SA, stearate; cer C2, ceramide-C2; FB1, fumonisin-B1; hyd per, hydrogen peroxide.

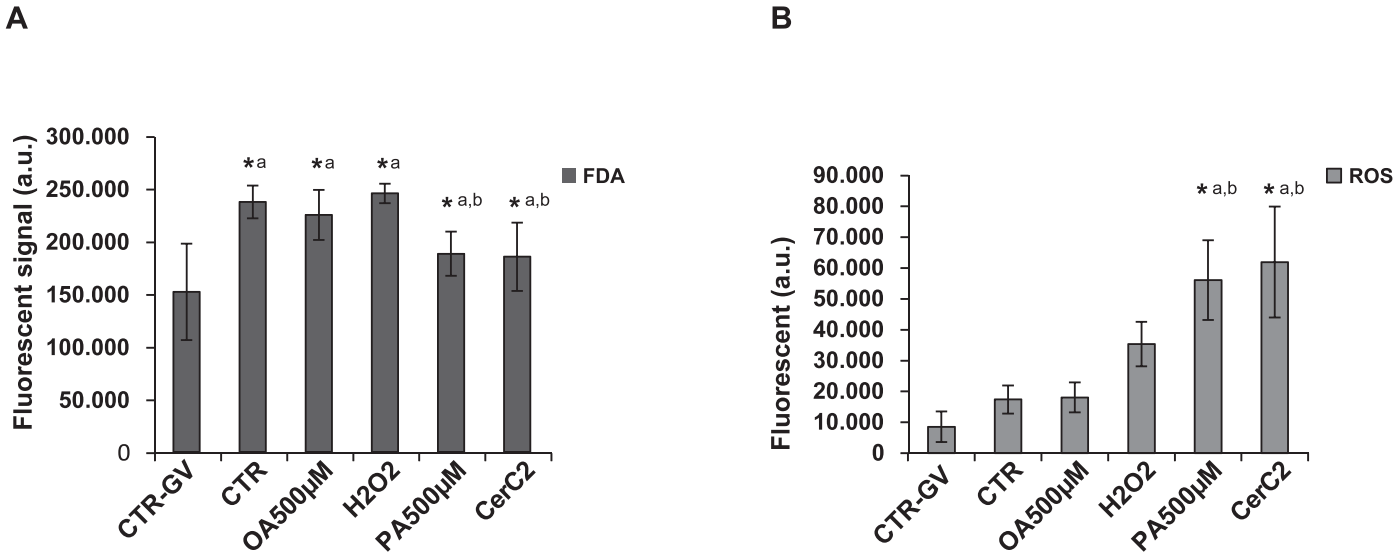

FIG. 6. Esterase activity quantitation and ROS formation before versus after in vitro maturation. Fluorescent signals of FDA (**A**) and DCHF-DA (**B**) quantitation in immature (CTR-GV) oocytes and in oocytes after maturation under control condition (CTR) or in maturation medium supplemented with either 250 μM OA, 500 μM PA, 100 μM ceramide-C2, or 1 mM hydrogen peroxide (H_2O_2). The analysis was performed on 20 live oocytes per treatment, and single oocyte fluorescent signals were measured as explained in *Materials and Methods*. Statistical analysis was performed using one-way ANOVA, and $*P < 0.05$ were considered significant. Index a is for significant effects when compared to the CTR-GV condition, and index b is for significant effects when compared to the control condition. CTR-GV, control germinal vesicle; CTR, control; OA, oleate; PA, palmitate; SA, stearate; cer C2, ceramide-C2.

(DCHF-DA) and chromatin (TO-PRO-3) as well as being immune labeled for perilipin-2 (Fig. 7). In the presence of PA or ceramide-C2, ROS production was always in the vicinity of LDs (Fig. 7A) as confirmed by the correlation analysis (Fig. 7B). This indicates that LDs or LD-associated structures (such as endoplasmic reticulum or mitochondria) may be involved in the observed ROS formation. Coclustering of LDs and ROS production was consistent in the entire oocyte volume as shown by the three-dimensional reconstruction of the COCs (see Fig. 8 and Supplemental Movie S1), and the correlation coefficients of ROS and perilipin-2 fluorescent signal increased in oocytes treated with PA or ceramide-C2 (Fig. 7B). In line with the noted detrimental effects of PA and ceramide-C2, we confirmed that these two conditions caused cumulus deterioration, in contrast to a normal expansion under control conditions (in the absence or presence of OA) (Fig. 7, C and D).

TABLE 1. ROS accumulation and morphological analysis of cumulus cells in matured COCs.[a]

Experimental group[b]	ROS positivity (%)[c]	Cumulus deterioration (%)[c]
Control (18)	33.3	27.8
OA 250 μM (14)	28.6	28.6
OA 500 μM (16)	25.0	12.5
PA 250 μM (12)	83.3*	58.3
PA 500 μM (16)	93.8*	75.0*
PA 500 μM + FB1 (12)	33.3	33.3
PA + OA 500 μM (18)	55.6	38.9
SA 250 μM (12)	50.0	50.0
SA 500 μM (12)	71.4*	57.1
SA 500 μM + FB1 (16)	25.0	25.0
SA + OA 500 μM (12)	66.7	66.7
Ceramide-C2 100 μM (18)	100*	88.9*
Hydrogen peroxide 1 mM (20)	100*	81.8*

[a] For all oocytes, irrespective of treatment, the percentage of COCs with positive DCHF-DA staining in the oocyte (ROS positive) was correlated with signs of cumulus damage in three independent experiments. Chi-square test was performed in order to compare the percentages of ROS positivity ($\chi 2 = 51.5$; $P < 0.005$) and percentage of cumulus deterioration ($\chi 2 = 55.2$; $P < 0.005$) among the different experimental conditions. Samples treated with hydrogen peroxide and ceramide-C2 were considered as positive controls (df = 10). Furthermore, on each individual COC, ROS formation and cumulus damage was highly correlated (Spearman rho correlation of 0.793, n = 200, $P < 0.0001$).

[b] The amount of COCs observed (value between parentheses) are indicated per each treatment group.

[c] Percentages of ROS-positive oocytes are correlated with percentages of cumulus deterioration.

* The asterisks indicate the conditions in which significant induction of either ROS formation and/or cumulus deterioration was observed when compared to control conditions after Bonferroni correction ($P < 0.05$; for exact P values see Supplemental Table S2).

PA and Ceramide-C2 Induce Mitochondrial Membrane Damage

To understand the role of FAs and ceramides in ROS production during in vitro maturation of COCs, the effects on mitochondrial integrity of maturing COCs were evaluated (Fig. 9). Saponin, a specific plasma membrane detergent, is effective in disrupting plasma membrane yet it leaves mitochondria unaffected [50]. Saponin thus can be used to discriminate between intact (not labeled) from deteriorated (labeled) mitochondria because labeling of the inner mitochondrial membrane enzyme COX IV is only permitted in deteriorated mitochondria. COCs preloaded with DCHF-DA were exposed to OA, PA, or ceramide-C2 and immune stained for COX IV (Fig. 9A). In saponin-permeabilized COCs, COX IV staining was absent in control or under OA conditions (Fig. 9A). In contrast, PA and more profoundly ceramide-C2 additions did induce damage of the mitochondrial membranes of COCs, allowing the immune labeling of COX IV, especially in cumulus cells (Fig. 9A). COCs permeabilized with Triton X-100, a nonselective detergent, showed COX IV immune fluorescent signal under the four analyzed conditions (Fig. 9A, right panels). In line with this, Western blot analysis of cumulus cells (Fig. 9B) and denuded oocytes (Fig. 9C) confirmed the presence of comparable amounts of COX-IV under the different treatments.

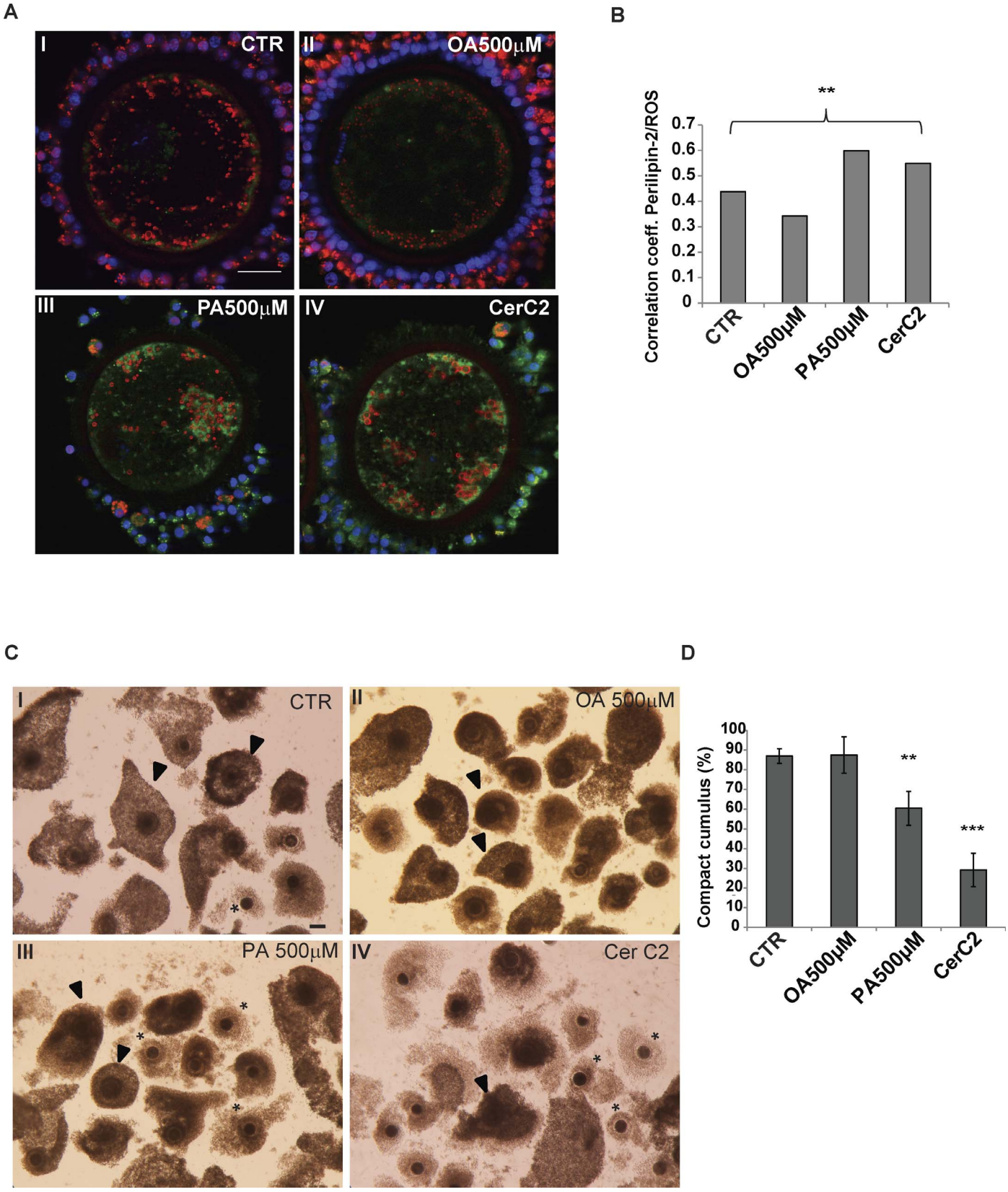

FIG. 7. High correlation between LD and ROS formation coincides with cumulus deterioration in presence of PA or ceramide-C2. **A**) Immune labeling of perilipin-2 (red), labeling of ROS-oxidized DCHF-DA (green), and labeling of DNA with TO-PRO-3 (blue) of COCs matured under four conditions: control (CTR) (**I**); with 500 μM OA (**II**); with 500 μM PA (**III**); or with 100 μM ceramide-C2 (Cer C2) (**IV**). Bar = 20 μm. **B**) Correlation coefficient (Spearman rho) and statistical analysis of fluorescent signals for perilipin-2 and ROS were performed with SPSS. The ratio of ROS and perilipin-2 signals within a grid of rectangular region of interest (ROI) in the oocyte images were measured and used to determine correlation between ROS accumulation and LDs. The correlation between the two fluorescent signals within each group is significant at $^{**}P \leq 0.01$ under these conditions. **C**, **D**) Morphologic analysis of cumulus morphology after 23 h of in vitro maturation under control condition or under different treatments. **C**) Light microscopy images of COCs with

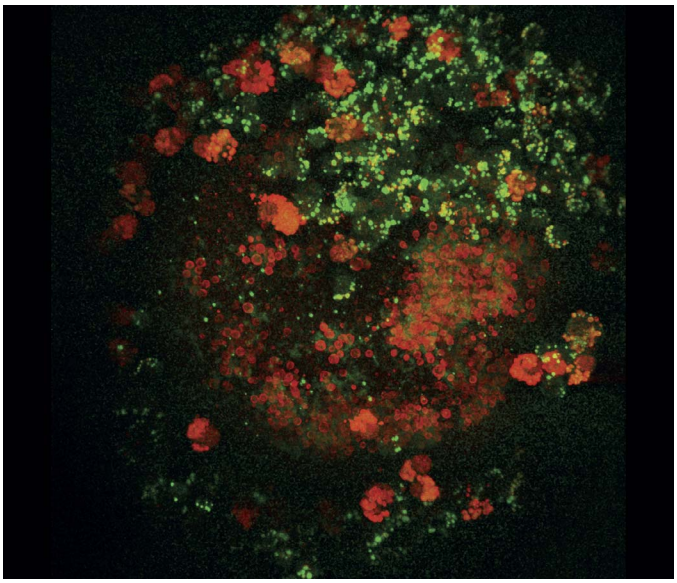

FIG. 8. Still for Supplemental Movie S1. Three-dimensional impression of LD localization versus ROS accumulation. Confocal imaging of one representative oocyte that was partially surrounded by its cumulus cells matured in the presence of 500 μM PA for 23 h. LDs are immune labeled for perilipin-2 (red) while ROS was detected by oxidation of DCHF-DA (green). For the still of this figure, an overlay of all individual stacks imaged is represented. For the video, sequential stacks taken through the oocyte show that the ROS signal is always present in the surrounding of the LDs pool. Each grid square has a width of 15 μm and a height of 15 μm.

PA and Ceramide-C2 Activate Apoptosis in Cumulus Cells of Maturing COCs

Activation of caspase-3, a key event in the induction of apoptosis [51], was investigated to understand the final outcome of PA-mediated mitochondrial deterioration. Lysates were made from denuded oocytes and their corresponding cumulus cell layers after in vitro maturation of COCs under various conditions. The lysates were used to detect the active form of caspase-3 on Western blots. The induction of cleavage of caspase-3 (into its active form) is specific for cumulus cells and was observed in the presence of PA, SA, and ceramide-C2 (Fig. 10, A and B). PA-activated caspase-3 could be reversed by either OA or FB1 (Fig. 10A), indicating that PA-induced lipotoxic effects were mediated via ceramide formation, resulting in a concerted action involving mitochondrial damage, ROS production, caspase-3 activation, and cumulus cell apoptosis. As a result, the deteriorating cumulus cell layer became incapable of protecting the oocyte from its harmful environment. In fact, when the cumulus protection was distorted by partial or total removal of the cumulus cell layers, spontaneous ROS formation in the absence of FA stress occurred (see Supplemental Fig. S4).

DISCUSSION

In the current study, the analysis of in vitro maturation of COCs that are exposed to various FAs was used to determine how the cumulus protects the oocyte from lipotoxic effects. Before discussing the outcome of this study, we should inform the reader about an intrinsic limitation of the in vitro model we designed. With this model, we aimed to mimic the specific FAs environment of the follicular fluid during in vivo maturation of the oocyte either under control or under high FAs concentration following short-fasting period conditions [12] or NEB [15–17]. The rationale was to investigate more in-depth the mechanisms via which various FAs may differently affect the lipid composition of COCs and whether or not the cumulus cell layer protects the maturing oocyte against lipotoxic consequences. However, in an in vivo model, a wide range of not here tested molecules, including metabolites such as beta hydroxybutyrate [12], could be considered. Moreover, hydrophilic and hydrophobic metabolites such as glucose and Chol have been reported to be filtered in a controlled way to become delivered to the oocyte by the cumulus-expanded matrix of the mouse [52]. Thus, beyond the FA-specific effects on oocyte maturation and cumulus function as reported here in vitro, the role of such other factors needs to be considered in future research. Consequently, not all the reproducible FA-specific effects reported here were found under short-term fasting in cows in vivo [12]. Also the short-term fasting model may not fully represent the metabolic imbalance and related FA stress in follicles of early postpartum cows. With the noted limitations of the chosen in vitro approach, we first showed an active role of the cumulus cells in modulating FA supply to the oocyte during in vitro maturation when functional coupling between the two cell types is necessary for the accomplishment of a metabolically favorable environment [6]. Removal of the cumulus cells caused rapid incorporation of FA into the neutral lipid of the oocyte. In the presence of cumulus cells, the administered FAs are predominantly stored in the LDs of cumulus cells, thus preventing a FA overload of the oocyte. The protective mechanism of FA storage in cumulus cells corresponds to in vivo observations on oocytes matured in the presence of elevated circulatory and follicular fluid FAs. The elevated circulatory FAs were due to fat mobilization from adipose tissues of short-term fasting cows. Under these conditions, FAs were stored in LDs of cumulus cells without affecting the maturation and quality of the oocyte [12]. These combined observations validate the physiological relevance of the in vitro system used in this study [52]. Second, maturing COCs were shown able to take up FAs from their environment and to incorporate them into the TG pool, as indicated by the increased amount of neutral lipids storage and by the enhanced immune labeling of the LD marker perilipin-2. In a previous study, we have shown that PA, and to a lower degree SA, caused reduced postfertilization developmental competence while OA did not have such an effect [19]. Concordantly, we show that PA and SA (but not OA) caused deterioration of the cumulus cell layer. Interestingly, similar lipotoxic effects have been observed in COCs in obese mouse oocytes [53], and adverse effects on lipid storage and cell functioning were described for oocyte maturation [54], fertilization [55], and early embryo development [32]. Lipidomic analysis of neutral lipids stored in COCs revealed that OA caused channeling of itself and of PA, and to a lesser extent SA, to neutral lipids and storage in LDs. This phenomenon has been described for somatic cells [26, 56] and has now been established for

panel numbers corresponding to maturation conditions as indicated for **A**. Solid arrows indicate COCs with properly expanded cumulus, asterisks mark COCs with deteriorating cumulus. Bar = 100 μm. **D**) Quantitative determination of oocytes with compact cumulus was performed on 572 COCs in total (n = 5, r > 130 for each maturation treatment). Asterisks indicates significant differences from the control (**$P \leq 0.01$ and ***$P \leq 0.001$). CTR, control; OA, oleate; PA, palmitate; SA, stearate; cer C2, ceramide-C2.

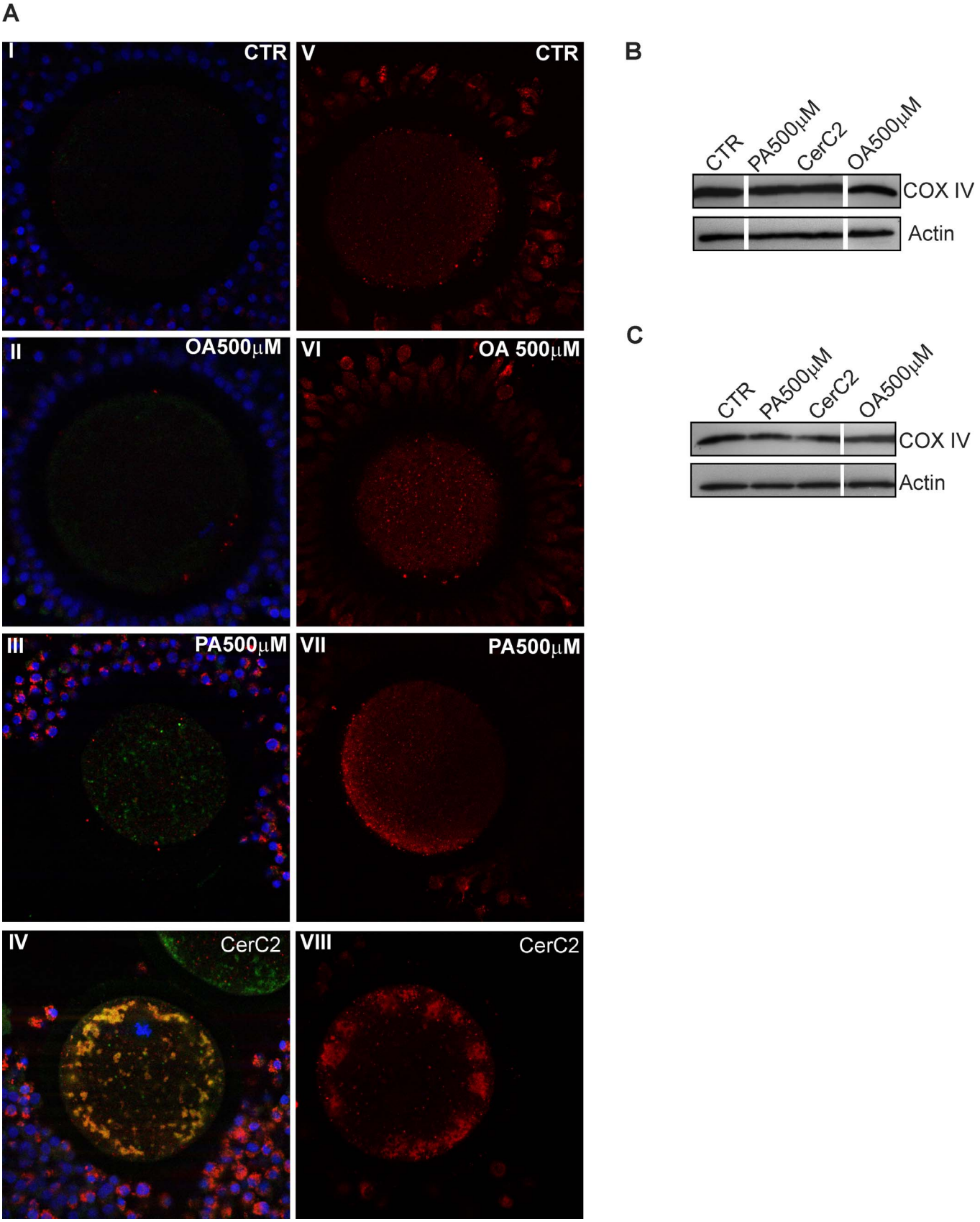

FIG. 9. PA and ceramide-C2 (Cer C2) induce mitochondrial membrane permeabilization in COCs. **A**) Left row: matured COCs permeabilized with saponin were triple stained with immune labeling for COX IV (red), with ROS-oxidized DCHF-DA (green), and with DNA staining using TO-PRO-3 (blue). Right row: COCs permeabilized with Triton X-100 and immune labeled for COX IV. Bar = 20 μm. Western blot analysis: immune detection of COX IV in cumulus cells (**B**) and oocytes (**C**). COCs matured in control condition and under different treatments were dissected and protein extracts from 50 oocyte per each lane and relative cumulus cells were loaded on a gel. Actin was used as loading control. CTR, control; OA, oleate; PA, palmitate; SA, stearate; cer C2, ceramide-C2.

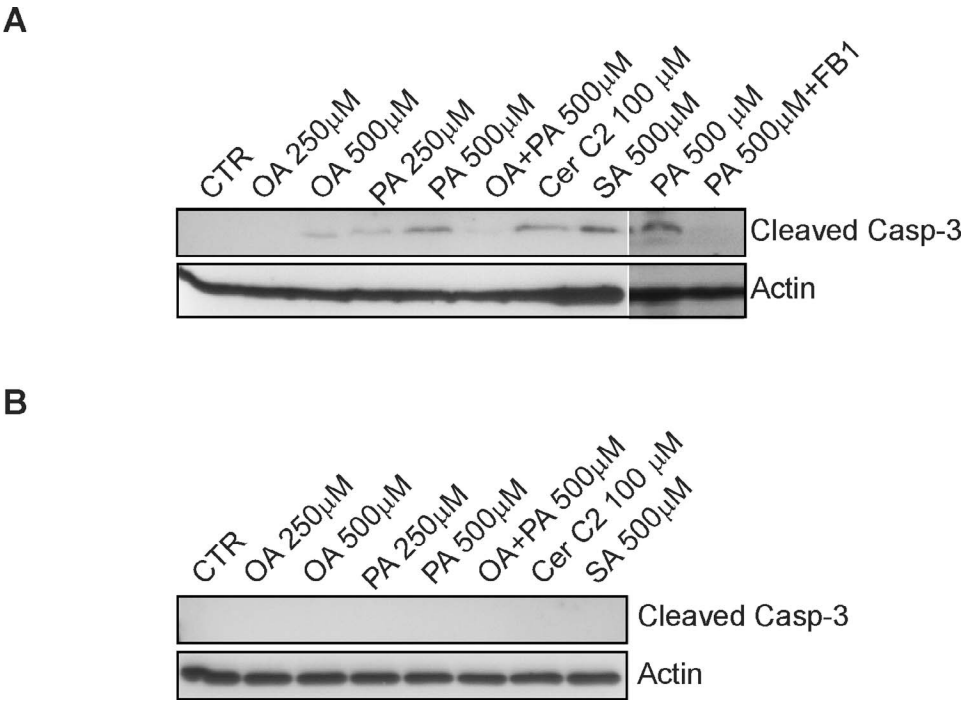

FIG. 10. Caspase 3 is activated in cumulus cells under PA exposure. Western blots show the immune detection of cleaved caspase-3 in cumulus cells (**A**) and oocytes (**B**). COCs matured under control condition and under different treatments were dissected, and protein extracts from 50 oocyte per each lane and relative cumulus cells were loaded on a gel. Actin was used as loading control. CTR, control; OA, oleate; PA, palmitate; SA, stearate; cer C2, ceramide-C2.

cumulus cells as well as for the oocyte under in vitro maturation conditions. In the cumulus cells, the administered FA were esterified to TG, DAG, and cholesteryl esters, and their respective molecular species were enriched accordingly. Interestingly, oocytes were much more sensitive to PA than SA or OA and only this FA caused a strong change in the neutral lipid profile of the oocyte. This profound effect is likely due to the cumulus deterioration caused by PA and not by the other FA treatments. Third, PA and SA (but not OA) exposure induced de novo ceramide synthesis (especially ceramide-C16). Anyway, only high concentrations of PA induced concomitant ceramide level increases, mitochondrial damage, ROS formation, and caspase-3 activation in cumulus cells. Under these conditions, partial disruption of the cumulus cell layer became manifest that essentially terminated the protective role of the cumulus cell layer surrounding the oocyte. These observations are consistent with the finding that an intact cumulus cell layer always correlated with lower ROS accumulation in the oocyte, suggesting a significant role of cumulus cells in protecting the oocyte from lipotoxic effects. An indirect effect of FB1 or ceramide-C2 by affecting neutral lipid storage was ruled out by lipidomic analysis, showing no effect on neutral lipid composition of cumulus cell layers and of oocytes. This supports the hypothesis made above, namely that ceramide synthesis causes the lipotoxic effects while the storage of lipids in LDs is not involved in the adverse effects of administered FAs [26].

Fourth, PA and to a lesser extent SA (but not OA) exposure also led to ROS production in the oocyte in the proximity of LDs. Ceramide-C2 treatment had similar but even more dramatic effects on the COCs in terms of ROS accumulation, ROS localization, and cumulus deterioration. In addition, ceramide-C2 treatment did cause a clustering of LDs inside the oocytes but did not cause an increase the neutral lipid content in cumulus cells and oocytes compared to control. The possibility that the emerging ROS (both in cumulus and in unprotected oocytes) are formed through leakage of electrons from the inner mitochondrial membrane during oxidative phosphorylation and ATP generation [57] should be further investigated. Wu et al. [32] revealed that lipotoxicity resulted in impaired pentraxin-3 secretion and related endoplasmic reticulum stress that altered the mitochondrial potential and consequently led to increased free radical formation. In line with this, the current study shows that ROS formation in either PA- or ceramide-C2-exposed oocytes occurred in every case in proximity to LDs and was limited to the cortex area (just under the oolemma). This finding may relate to the higher cytosolic FA levels in close proximity to mitochondria, which may cause more intense lipotoxic stress. How LDs, ceramides, and ROS production are mechanistically coupled remains to be determined. Specific contacts have been described bringing together the endoplasmic reticulum, mitochondria, and LDs [32, 54, 58]. The endoplasmic reticulum is the specific site for de novo ceramide formation, and in this study, FB1inhibited PA-induced ceramide formation, mitochondrial damage, ROS production, and caspase-3 activation. The close proximity of the organelles involved suggests that specific contact sites may be involved in special organization of sequential signaling events. Of specific note, ceramide and ROS formation within the oocyte did not lead to caspase activation. This suggests that the mature oocyte, being arrested at the metaphase of the second meiotic division, lacks the machinery to induce apoptosis as has been reported before [59]. Besides lacking machinery, cumulus cells may also be more susceptible to ROS formation and consequent initiation of lipid peroxidation cascades [60] due to the elevated concentrations of highly unsaturated FA, particularly docosahexaenoic acid (22:6) (data not shown).

Besides the degenerative effects of ceramides on cumulus cells, we also noted increased levels of glucosylceramides.

Glycosphingolipids are reported to be involved in alterations in cell surface properties, directly or indirectly influencing adhesive properties of the cell surface [61, 62]. Future research should elucidate whether the enhanced formation of glucosylceramides under lipotoxic-inducing conditions in COCs relates to alterations in contact sites between these cells. Cumulus cell expansion is a hallmark for oocyte maturation, and aberrations of the bidirectional oocyte-cumulus signaling may affect oocyte developmental competence and embryo outcomes [63]. The degree of cumulus expansion and/or its intactness reflects the oocyte's developmental competence and is often used as a criterion for oocyte selection [64]. The present study has revealed a novel role of OA in cumulus cells in that it protects the oocyte from FA-induced lipotoxic effects. Beside the veterinary relevance for high-yielding dairy cows and induced fertility problems [65], this knowledge is also relevant for human medicine. Recent studies have correlated maternal overweight and obesity with altered follicular fluid lipid composition and lipid accumulation as well as with suboptimal fertility [33, 66].

ACKNOWLEDGMENT

The authors thank H.T.A. van Tol and E.J. Schoevers for their technical assistance and for help in the collection of the oocytes and E.M. van't Veld for her support during the confocal microscopy sessions.

REFERENCES

1. Wu B, Ignotz GG, Currie WB, Yang X. Temporal distinctions in the synthesis and accumulation of proteins by oocytes and cumulus cells during maturation in vitro of bovine oocytes. Mol Reprod Dev 1996; 45: 560–565.
2. Krisher RL. The effect of oocyte quality on development. J Anim Sci 2004; 82:E14–E23.
3. Kimura N, Hoshino Y, Totsukawa K, Sato E. Cellular and molecular events during oocyte maturation in mammals: molecules of cumulus-oocyte complex matrix and signalling pathways regulating meiotic progression. Soc Reprod Fertil Suppl 2007; 63:327–342.
4. Lonergan P, Rizos D, Gutierrez-Adan A, Fair T, Boland MP. Oocyte and embryo quality: effect of origin, culture conditions and gene expression patterns. Reprod Domest Anim 2003; 38:259–267.
5. Eppig JJ. The relationship between cumulus cell-oocyte coupling, oocyte meiotic maturation, and cumulus expansion. Dev Biol 1982; 89:268–272.
6. Tanghe S, Van Soom A, Nauwynck H, Coryn M, de Kruif A. Minireview: functions of the cumulus oophorus during oocyte maturation, ovulation, and fertilization. Mol Reprod Dev 2002; 61:414–424.
7. Huang Z, Wells D. The human oocyte and cumulus cells relationship: new insights from the cumulus cell transcriptome. Mol Hum Reprod 2010; 16: 715–725.
8. Buccione R, Schroeder AC, Eppig JJ. Interactions between somatic cells and germ cells throughout mammalian oogenesis. Biol Reprod 1990; 43: 543–547.
9. Wigglesworth K, Lee KB, O'Brien MJ, Peng J, Matzuk MM, Eppig JJ. Bidirectional communication between oocytes and ovarian follicular somatic cells is required for meiotic arrest of mammalian oocytes. Proc Natl Acad Sci U S A 2013; 110:E3723–E3729.
10. Biggers JD, Whittingham DG, Donahue RP. The pattern of energy metabolism in the mouse oocyte and zygote. Proc Natl Acad Sci U S A 1967; 58:560–567.
11. Thompson JG, Lane M, Gilchrist RB. Metabolism of the bovine cumulus-oocyte complex and influence on subsequent developmental competence. Soc Reprod Fertil Suppl 2007; 64:179–190.
12. Aardema H, Lolicato F, van de Lest CH, Brouwers JF, Vaandrager AB, van Tol HT, Roelen BA, Vos PL, Helms JB, Gadella BM. Bovine cumulus cells protect maturing oocytes from increased fatty acid levels by massive intracellular lipid storage. Biol Reprod 2013; 88:164.
13. Eppig JJ. Intercommunication between mammalian oocytes and companion somatic cells. Bioessays 1991; 13:569–574.
14. Gilchrist RB, Lane M, Thompson JG. Oocyte-secreted factors: regulators of cumulus cell function and oocyte quality. Hum Reprod Update 2008; 14:159–177.
15. Leroy JL, Opsomer G, Van Soom A, Goovaerts IG, Bols PE. Reduced fertility in high-yielding dairy cows: are the oocyte and embryo in danger? Part I. The importance of negative energy balance and altered corpus luteum function to the reduction of oocyte and embryo quality in high-yielding dairy cows.Reprod Domest Anim 2008; 43:612–622.
16. Leroy JL, Van Soom A, Opsomer G, Goovaerts IG, Bols PE. Reduced fertility in high-yielding dairy cows: are the oocyte and embryo in danger? Part II. Mechanisms linking nutrition and reduced oocyte and embryo quality in high-yielding dairy cows.Reprod Domest Anim 2008; 43: 623–632.
17. Leroy JL, Van Soom A, Opsomer G, Bols PE. The consequences of metabolic changes in high-yielding dairy cows on oocyte and embryo quality. Animal 2008; 2:1120–1127.
18. Leroy JL, Vanholder T, Mateusen B, Christophe A, Opsomer G, de Kruif A, Genicot G, Van Soom A. Non-esterified fatty acids in follicular fluid of dairy cows and their effect on developmental capacity of bovine oocytes in vitro. Reproduction 2005; 130:485–495.
19. Aardema H, Vos PL, Lolicato F, Roelen BA, Knijn HM, Vaandrager AB, Helms JB, Gadella BM. Oleic acid prevents detrimental effects of saturated fatty acids on bovine oocyte developmental competence. Biol Reprod 2011; 85:62–69.
20. Van Hoeck V, Sturmey RG, Bermejo-Alvarez P, Rizos D, Gutierrez-Adan A, Leese HJ, Bols PE, Leroy JL. Elevated non-esterified fatty acid concentrations during bovine oocyte maturation compromise early embryo physiology. PLoS One 2011; 6:e23183.
21. Homa ST, Racowsky C, McGaughey RW. Lipid analysis of immature pig oocytes. J Reprod Fertil 1986; 77:425–434.
22. Cetica P, Pintos L, Dalvit G, Beconi M. Activity of key enzymes involved in glucose and triglyceride catabolism during bovine oocyte maturation in vitro. Reproduction 2002; 124:675–681.
23. Fair T, Hulshof SC, Hyttel P, Greve T, Boland M. Oocyte ultrastructure in bovine primordial to early tertiary follicles. Anat Embryol (Berl) 1997; 195:327–336.
24. Ferguson EM, Leese HJ. A potential role for triglyceride as an energy source during bovine oocyte maturation and early embryo development. Mol Reprod Dev 2006; 73:1195–1201.
25. Dunning KR, Cashman K, Russell DL, Thompson JG, Norman RJ, Robker RL. Beta-oxidation is essential for mouse oocyte developmental competence and early embryo development. Biol Reprod 2010; 83: 909–918.
26. Listenberger LL, Han X, Lewis SE, Cases S, Farese RV Jr, Ory DS, Schaffer JE. Triglyceride accumulation protects against fatty acid-induced lipotoxicity. Proc Natl Acad Sci U S A 2003; 100:3077–3082.
27. Kim H, Ye J. Cellular responses to excess fatty acids: focus on ubiquitin regulatory X domain-containing protein 8. Curr Opin Lipidol 2014; 25: 118–124.
28. Shimabukuro M, Ohneda M, Lee Y, Unger RH. Role of nitric oxide in obesity-induced beta cell disease. J Clin Invest 1997; 100:290–295.
29. Schaffer JE. Lipotoxicity: when tissues overeat. Curr Opin Lipidol 2003; 14:281–287.
30. Listenberger LL, Ory DS, Schaffer JE. Palmitate-induced apoptosis can occur through a ceramide-independent pathway. J Biol Chem 2001; 276: 14890–14895.
31. Colombini M. Membrane channels formed by ceramide. Handb Exp Pharmacol 2013; 215:109–126.
32. Wu LL, Russell DL, Norman RJ, Robker RL. Endoplasmic reticulum (ER) stress in cumulus-oocyte complexes impairs pentraxin-3 secretion, mitochondrial membrane potential (DeltaPsi m), and embryo development. Mol Endocrinol 2012; 26:562–573.
33. Jungheim ES, Macones GA, Odem RR, Patterson BW, Lanzendorf SE, Ratts VS, Moley KH. Associations between free fatty acids, cumulus oocyte complex morphology and ovarian function during in vitro fertilization. Fertil Steril 2011; 95:1970–1974.
34. Van de Velde H, Nagy ZP, Joris H, De Vos A, Van Steirteghem AC. Effects of different hyaluronidase concentrations and mechanical procedures for cumulus cell removal on the outcome of intracytoplasmic sperm injection. Hum Reprod 1997; 12:2246–2250.
35. Wang E, Norred WP, Bacon CW, Riley RT, Merrill AH Jr. Inhibition of sphingolipid biosynthesis by fumonisins. Implications for diseases associated with Fusarium moniliforme. J Biol Chem 1991; 266: 14486–14490.
36. Yuzefovych L, Wilson G, Rachek L. Different effects of oleate vs. palmitate on mitochondrial function, apoptosis, and insulin signaling in L6 skeletal muscle cells: role of oxidative stress. Am J Physiol Endocrinol Metab 2010; 299:E1096–E1105.
37. Morado SA, Cetica PD, Beconi MT, Dalvit GC. Reactive oxygen species in bovine oocyte maturation in vitro. Reprod Fertil Dev 2009; 21:608–614.
38. Jones TR, Kang IH, Wheeler DB, Lindquist RA, Papallo A, Sabatini DM,

Golland P, Carpenter AE. CellProfiler Analyst: data exploration and analysis software for complex image-based screens. BMC Bioinformatics 2008; 9:482.
39. Grealy M, Diskin MG, Sreenan JM. Protein content of cattle oocytes and embryos from the two-cell to the elongated blastocyst stage at day 16. J Reprod Fertil 1996; 107:229–233.
40. Bligh EG, Dyer WJ. A rapid method of total lipid extraction and purification. Can J Biochem Physiol 1959; 37:911–917.
41. Rouser G, Fkeischer S, Yamamoto A. Two dimensional then layer chromatographic separation of polar lipids and determination of phospholipids by phosphorus analysis of spots. Lipids 1970; 5:494–496.
42. Brouwers JF, Gadella BM, van Golde LM, Tielens AG. Quantitative analysis of phosphatidylcholine molecular species using HPLC and light scattering detection. J Lipid Res 1998; 39:344–353.
43. Smith CA, Want EJ, O'Maille G, Abagyan R, Siuzdak G. XCMS: processing mass spectrometry data for metabolite profiling using nonlinear peak alignment, matching, and identification. Anal Chem 2006; 78: 779–787.
44. Stacklies W, Redestig H, Scholz M, Walther D, Selbig J. pcaMethods—a bioconductor package providing PCA methods for incomplete data. Bioinformatics 2007; 23:1164–1167.
45. Schaffer JE, Lodish HF. Expression cloning and characterization of a novel adipocyte long chain fatty acid transport protein. Cell 1994; 79: 427–436.
46. Faergeman NJ, DiRusso CC, Elberger A, Knudsen J, Black PN. Disruption of the Saccharomyces cerevisiae homologue to the murine fatty acid transport protein impairs uptake and growth on long-chain fatty acids. J Biol Chem 1997; 272:8531–8538.
47. Straub BK, Gyoengyoesi B, Koenig M, Hashani M, Pawella LM, Herpel E, Mueller W, Macher-Goeppinger S, Heid H, Schirmacher P. Adipophilin/perilipin-2 as a lipid droplet-specific marker for metabolically active cells and diseases associated with metabolic dysregulation. Histopathology 2013; 62:617–631.
48. Mu YM, Yanase T, Nishi Y, Tanaka A, Saito M, Jin CH, Mukasa C, Okabe T, Nomura M, Goto K, Nawata H. Saturated FFAs, palmitic acid and stearic acid, induce apoptosis in human granulosa cells. Endocrinology 2001; 142:3590–3597.
49. Lu ZH, Mu YM, Wang BA, Li XL, Lu JM, Li JY, Pan CY, Yanase T, Nawata H. Saturated free fatty acids, palmitic acid and stearic acid, induce apoptosis by stimulation of ceramide generation in rat testicular Leydig cell. Biochem Biophys Res Commun 2003; 303:1002–1007.
50. Willingham M. An Atlas of Immunofluorescence in Cultured Cells. London: Academic Press; 1985.
51. Namura S, Zhu J, Fink K, Endres M, Srinivasan A, Tomaselli KJ, Yuan J, Moskowitz MA. Activation and cleavage of caspase-3 in apoptosis induced by experimental cerebral ischemia. J Neurosci 1998; 18: 3659–3668.
52. Dunning KR, Watson LN, Sharkey DJ, Brown HM, Norman RJ, Thompson JG, Robker RL, Russell DL. Molecular filtration properties of the mouse expanded cumulus matrix: controlled supply of metabolites and extracellular signals to cumulus cells and the oocyte. Biol Reprod 2012; 87:89.
53. Wu LL, Norman RJ, Robker RL. The impact of obesity on oocytes: evidence for lipotoxicity mechanisms. Reprod Fertil Dev 2011; 24:29–34.
54. Yang X, Dunning KR, Wu LL, Hickey TE, Norman RJ, Russell DL, Liang X, Robker RL. Identification of perilipin-2 as a lipid droplet protein regulated in oocytes during maturation. Reprod Fertil Dev 2010; 22: 1262–1271.
55. Wu LL, Dunning KR, Yang X, Russell DL, Lane M, Norman RJ, Robker RL. High-fat diet causes lipotoxicity responses in cumulus-oocyte complexes and decreased fertilization rates. Endocrinology 2010; 151: 5438–5445.
56. Henique C, Mansouri A, Fumey G, Lenoir V, Girard J, Bouillaud F, Prip-Buus C, Cohen I. Increased mitochondrial fatty acid oxidation is sufficient to protect skeletal muscle cells from palmitate-induced apoptosis. J Biol Chem 2010; 285:36818–36827.
57. West AP, Shadel GS, Ghosh S. Mitochondria in innate immune responses. Nat Rev Immunol 2011; 11:389–402.
58. Brasaemle DL, Wolins NE. Packaging of fat: an evolving model of lipid droplet assembly and expansion. J Biol Chem 2012; 287:2273–2279.
59. Rubio Pomar FJ, Roelen BA, Slot KA, van Tol HT, Colenbrander B, Teerds KJ. Role of Fas-mediated apoptosis and follicle-stimulating hormone on the developmental capacity of bovine cumulus oocyte complexes in vitro. Biol Reprod 2004; 71:790–796.
60. Jones R, Mann T, Sherins R. Peroxidative breakdown of phospholipids in human spermatozoa, spermicidal properties of fatty acid peroxides, and protective action of seminal plasma. Fertil Steril 1979; 31:531–537.
61. Lavie Y, Cao H, Bursten SL, Giuliano AE, Cabot MC. Accumulation of glucosylceramides in multidrug-resistant cancer cells. J Biol Chem 1996; 271:19530–19536.
62. Treyer A, Musch A. Hepatocyte polarity. Compr Physiol 2013; 3: 243–287.
63. Yeo CX, Gilchrist RB, Lane M. Disruption of bidirectional oocyte-cumulus paracrine signaling during in vitro maturation reduces subsequent mouse oocyte developmental competence. Biol Reprod 2009; 80: 1072–1080.
64. Blondin P, Sirard MA. Oocyte and follicular morphology as determining characteristics for developmental competence in bovine oocytes. Mol Reprod Dev 1995; 41:54–62.
65. Leroy JL, Rizos D, Sturmey R, Bossaert P, Gutierrez-Adan A, Van Hoeck V, Valckx S, Bols PE. Intrafollicular conditions as a major link between maternal metabolism and oocyte quality: a focus on dairy cow fertility. Reprod Fertil Dev 2011; 24:1–12.
66. Valckx SD, De Pauw I, De Neubourg D, Inion I, Berth M, Fransen E, Bols PE, Leroy JL. BMI-related metabolic composition of the follicular fluid of women undergoing assisted reproductive treatment and the consequences for oocyte and embryo quality. Hum Reprod 2012; 27:3531–3539.